Comparison of acoustic pulse propagation between scale-model measurements and three-dimensional simulation over real-life urban topography

Takuya OSHIMA[1]; Takashi ISHIZUKA[2]; Takahide KAMIJO[3]

[1] Niigata University, Japan

[2] Institute of Technology, Shimizu Corporation, Japan

[3] Niigata University (Present affiliation: NTT Facilities Chuo, Inc.), Japan

ABSTRACT

In Inter-Noise 2013, the authors presented a study comparing acoustic propagation measurements over a 1:100 scale model of a real-life urban topography and large-scale three-dimensional finite-difference time-domain simulations. The results were presented in octave-band sound pressure levels. As a sequel to the 2013 paper, this paper compares the results in time domain. The waveforms of acoustic pulse propagation are computed by inverse filtering the source responses of an electric spark generator of the measurements and a Gaussian pulse of the simulation. The results show excellent matches at line-of-sight and single diffraction receiver positions in overall waveform structure, especially in arrival times of the diffracted and reflected pulses. The arrival time matched even after 0.7 s of traveling time. However, major discrepancies are observed at a receiver position which is affected by a combination of double diffraction and multiple reflections and positions affected by deep triple diffractions. Furthermore, in such positions, the simulated waveforms are found to have more energy in higher frequency. The discrepancies are possibly attributed to the use of rigid surfaces in the simulation and the lack of air absorption correction in the measured data processing.

Keywords: Urban acoustic propagation, Scale-model experiments, Finite-difference time-domain simulation
I-INCE Classification of Subjects Number(s): 24.4, 24.5

1. INTRODUCTION

Prediction of sound propagation over a complex real-life urban topography has been a challenging problem that is of interest in many aspects and has many practical applications. In addition to engineering models that has been used for a long time, time-domain acoustic simulations are becoming viable options for such problems. The time-domain simulations have advantages over engineering models in accurately modeling time-domain wave phenomena such as interference, diffraction and multiple reflections. However, the limiting factors in performing time-domain simulations have been the computer resources required to accommodate the vast computational domain size and the absence of a geometry reproduction technique of the topography. Although the frequency range still remains low, such simulations are actively attempted following recent advances of computer performances and a topography reproduction technique using digital geographic datasets. Now, validation of the simulation results are of interest. Albert *et al.* (1) compared the results of two-dimensional simulations over a full-scale artificial village with experimental measurements up to approximately the 200 Hz frequency range. Heimann (2) performed a low-frequency three-dimensional simulation of approximately 10 Hz over a natural terrain. The results were validated with measured point-to-point level differences. Oshima *et al.* (3) performed three-dimensional finite-difference time-domain (FDTD) simulations over a dense urban topography of approximately 200 Hz. Validation of the FDTD implementation was performed by comparisons with theoretical free-field solutions. Mehra *et al.* (4) compared a three-dimensional adaptive rectangular decomposition (ARD) simulation with the aforementioned full-scale experiment by Albert *et al.* (1) by the waveforms which contain up to the 500 Hz component.

As seen from the previous works, until recently no study has reproduced complex urban topography from digital geographic datasets and compared measurements and three-dimensional simulations of sound prop-

[1] oshima@eng.niigata-u.ac.jp
[2] ishiduka@shimz.co.jp
[3] kamijo23@ntt-f.co.jp

agation over the topography. At Inter-Noise 2013, the authors presented such a study comparing acoustic propagation measurements over a 1:100 scale model of a real-life urban area and a three-dimensional FDTD simulation over the same urban geometry in full scale (5). Overall results were presented in octave bands because expected main application was environmental noise prediction. However, for the time-domain simulations, comparing waveforms is a more stringent test as it requires good agreement between the amplitudes and phases of the measured and simulated waveforms (4). The time-domain behavior of urban sound propagation has also practical importance to acoustic source localization using time reversal processing (6).

As a sequel to (5), this paper aims to provide a more in-depth view of the measurement and simulation results in time domain. The waveforms of acoustic pulse propagation are computed by inverse filtering the source responses of an electric spark generator of the measurements and a Gaussian pulse of the simulation. The receiver positions are categorized by line-of-sight, diffracted and multiply reflected source-receiver propagation paths. In each category, comparisons are made through arrival times and amplitudes of diffracted and reflected acoustic pulses.

2. MEASUREMENT AND SIMULATION

2.1 Subject Urban Topography

The subject urban topography and the raw results of the measurement and simulation used in this study are excerpts of those used in our previous works (5, 7). The topography and settings are briefly given in this and the next subsection. See (5, 7) for more details.

The subject of the study is a 380 m×380 m area in Kanagawa, Japan, as shown in Figure 1(a). Remarks enclosed by boxes in the panel like SP are explained in Sections 2.2 and 3. The latitudes and longitudes of the southwest and northeast corners of the area are (35° 28′ 56″ N, 139° 37′ 2″ E) and (35° 29′ 8″ N, 139° 37′ 17″ E), respectively. For reconstruction of the topography and the building shapes, the following three types of datasets are used: a digital surface model (DSM) (8), a digital elevation model (8), and a building outline dataset (9). For simplicity of the scale-model creation, small detached houses are not included in the reconstructed geometry.

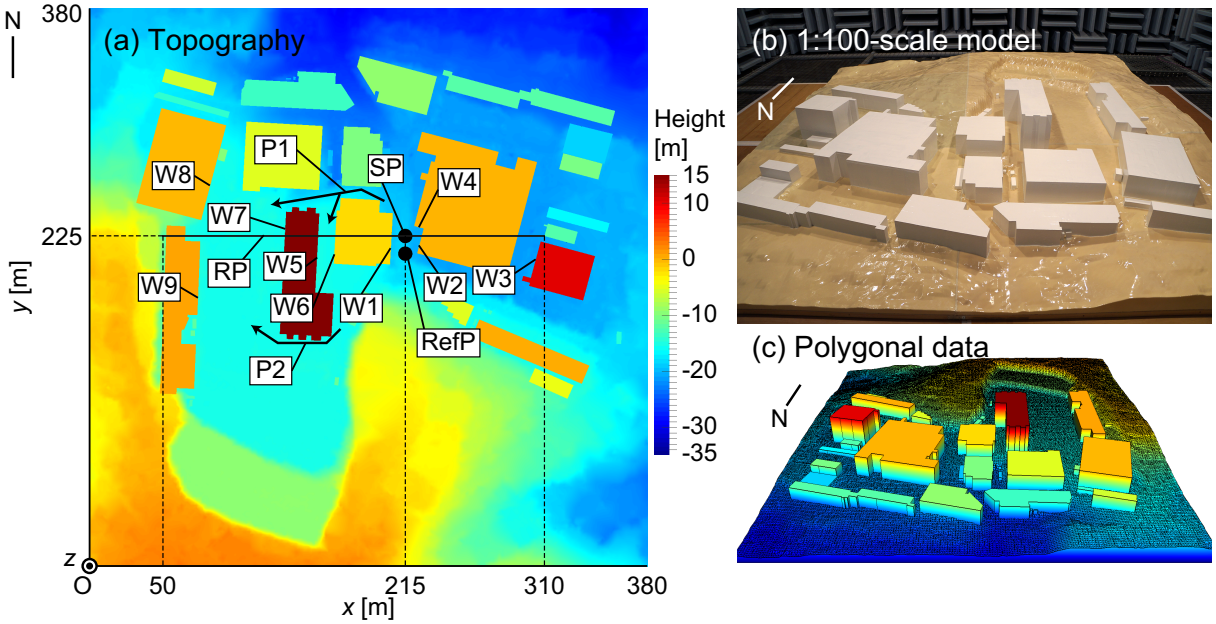

Figure 1 – (a) Topography of the subject area, sources and receivers. (b) 1:100 scale model used for the measurements. (c) Polygonal data used for the FDTD simulation. The gradation indicates height as in panel (a). Panels (a)–(c) are reproduced from (7).

From the datasets, the model used for the measurements is created on a scale of 1:100. The material of the model is resin foam with a hardening treatment of the terrain surface and acrylic coating of the building surfaces so that the surfaces are regarded as acoustically rigid. The complete model is shown in Figure 1(b). The input geometry for the simulation is created in full scale by applying the technique by Oshima *et al.* (10). The geometry is shown in Figure 1(c).

2.2 Measurement and Simulation Settings

Axes, a source, a receiver plane, a reference point, and their positions in full scale are shown in Figure 1(a). The coordinates are local ones that originate from the ground level of the southwest end of the subject area. The x, y, and z axes represent the eastward, northward, and upward directions, respectively. SP is the source, RP is the vertical receiver plane, RefP is the reference point. Of 378 receiver points taken on RP (5), 15 receivers named R1–R15 are selected and marked in Figure 2. The colors of the marks denote the number of diffractions required for propagating sound from SP to arrive at each receiver. At black points, line-of-sight (LOS) is obtained from SP (no diffraction). Other colors denote non-line-of-sight (NLOS) positions with red, green, and blue indicating single, double, and triple diffractions (NLOS-1, 2, and 3), respectively.

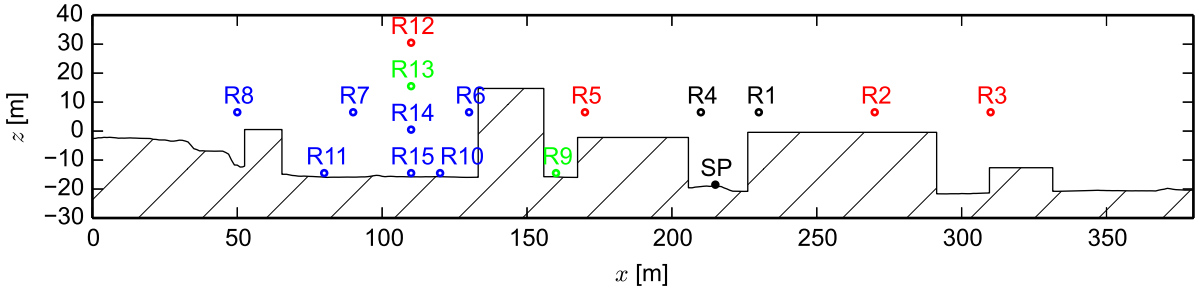

Figure 2 – Receiver positions on receiving plane RP. The receiver points marked in black, red, green, and blue denote that they are at LOS (line-of-sight), NLOS(non-line-of-sight)-1, 2, and 3 positions.

The measurements are taken in an anechoic room. An electric spark pulse generator is used as the sound source. With the recording sampling rate of 192 kHz, a set of waveforms of 4 499 samples are obtained for a single receiver point by a 1/4-inch microphone. Then, 25–32 mutually similar waveforms are chosen by correlative operations. Time synchronous averaging is performed on the chosen waveforms. To correct the variations in the acoustic powers of spark radiations, the amplitude of each waveform is normalized by the maximum amplitude of the acoustic pressure observed at reference point RefP during sampling of the waveform. The obtained waveforms are transformed to the full scale by stretching the temporal axis by a factor of 100. Hence, the sample rate in full scale is 1 920 Hz and the duration of a waveform with the 4 499 samples is 2.34 s.

For the simulation, an FDTD method is coded in C++ and applied to the simulation. The simulation is conducted in full scale. The speed of sound 339.6 m/s is calculated from the average temperatures of the scale-model measurements. The grid spacing, time step and simulated time duration are 0.1 m, 1.6×10^{-4} s (which corresponds to a sample rate of 6 250 Hz), and 4 s, respectively. The grid spacing yields a computational domain of $3\,760 \times 3\,760 \times 1\,400$ grid points. A perfectly matched layer (11) with a thickness of 20 grid points is added to the top and lateral boundaries of the computational domains of all cases. Of the duration of 4 s, the beginning 14 645 samples, which is consistent with the 2.34 s duration of the measurements, is used. The source is an initial Gaussian pressure pulse of full-width half-maximum 1 m. The boundary conditions of the terrain and building surfaces are rigid in all cases.

2.3 Source Responses and Signal Processing

The measurement of the source response and signal processing described in this subsection is newly introduced in this paper. Firstly, the source waveform of the spark pulse is obtained at a distance of 200 mm in the anechoic room in a free-field condition. Also, a simulation to obtain the waveform of the Gaussian pulse at a distance of 20 m from the center point of the pulse is run in a free-field condition. Figure 3 shows the waveforms and the frequency responses. Then, the waveforms obtained at the receivers are fast Fourier transformed to the frequency domain, inverse filtered by the respective source frequency responses using a Wiener filter with a constant assumed signal-to-noise ratio of 10^5, and inverse fast Fourier transformed to the time domain. The simulated waveforms are downsampled to a sample rate of 1 920.02 Hz during the inverse transformation. Since the Gaussian pulse used in the simulation does not contain frequency components over 500 Hz as shown in Figure 3(b), a linear-phase low-pass filter of cutoff frequency 500 Hz and depth −60 dB is applied to both measured and simulated waveforms. The low-pass filter is applied not only to the measured waveforms but also to the simulated waveforms to ensure that the same filter characteristic is convolved to the final waveforms. Furthermore, a linear-phase high-pass filter of cutoff frequency 20 Hz and depth −20 dB is applied to the measured and simulated waveforms to remove low-frequency trends induced by the inverse filtering.

Unlike the previous paper, air absorption is not corrected because its dependency to both time (propagation

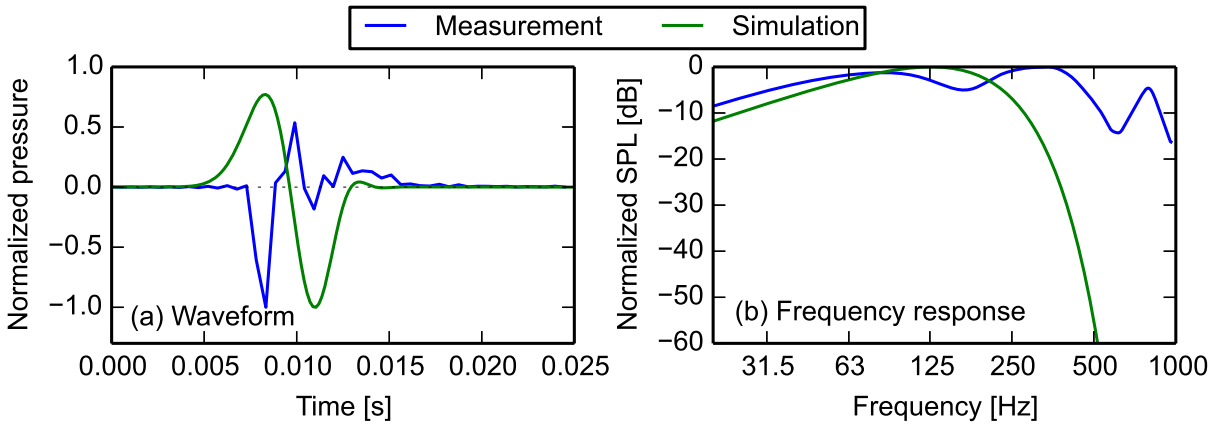

Figure 3 – Source responses.

distance divided by the speed of sound) and frequency did not fit well in the workflow of the signal processing.

3. RESULTS AND DISCUSSION

3.1 Visualization of the Simulation Result

The acoustic propagation obtained by the simulation is mapped to the building and ground surfaces and visualized as a sequential movie in a $3\,840 \times 2\,160$ pixel (4K) resolution. Figure 4 shows a snapshot at a time of 0.496 s of the movie but in a reduced resolution of $1\,920 \times 1\,080$ pixels. The acoustic propagation path analyses mentioned hereafter are performed using the movie.

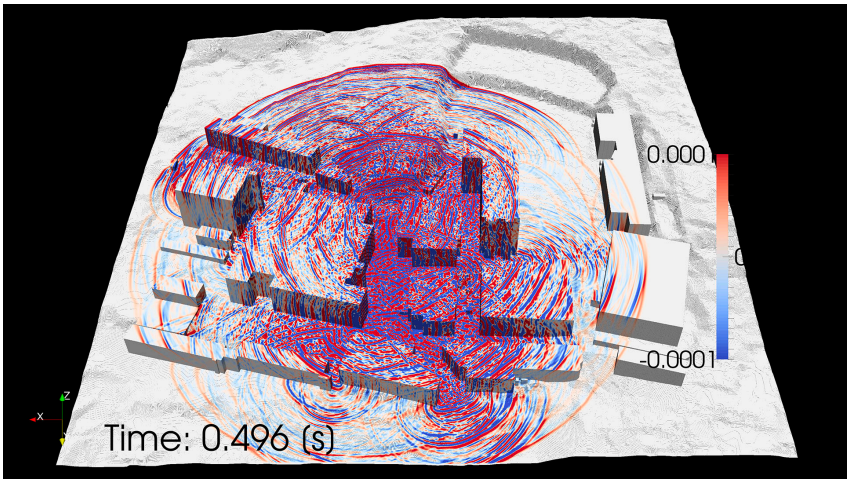

Figure 4 – Snapshot of visualized acoustic propagation at time 0.496 s. Red and blue colors denote positive and negative acoustic pressure.

3.2 R1–R3

Receivers R1–R3 are positioned in a row with a uniform spacing to study the effect of distance from SP in relatively simple geometry and the effects of shallow diffraction conditions of LOS and NLOS-1. The left panels of Figure 5 shows the waveforms of beginning 1 s at R1–R3. The upper blue and the lower green waveforms in each panel are the measured and simulated waveforms, respectively. The amplitude of each waveform is normalized by its maximum amplitude. Hence, the amplitudes cannot be directly compared between the measurements and simulation. The background color of each panel denote the number of diffractions of the propagation path between the source to the receiver. The white and pale red backgrounds denote LOS propagation and NLOS-1 propagation, respectively. The right panels of Figure 5 are the relative sound pressure levels (SPLs) calculated by cumulating the corresponding waveforms along the temporal axis and normalized by each total cumulative energy during the entire duration of 2.34 s. The color scheme is same as the left panels.

In the left panel of Figure 5(a) are the waveforms observed at R1, where LOS is barely obtained as seen

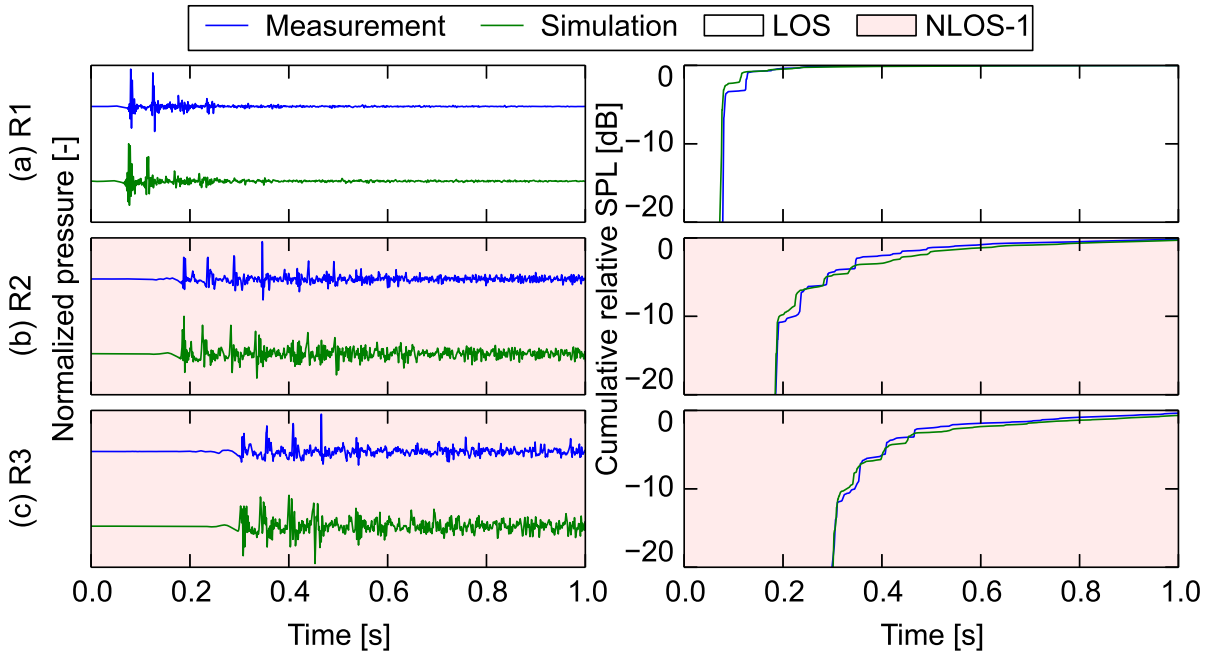

Figure 5 – (Left) waveforms and (right) cumulative relative SPLs at R1–R3.

from Figure 2. The the arrival times of the first arrival (direct pulse) matches between the measurement and simulation. However, for the second and onward arrivals, which are pulses multiply reflected by the building walls W1 and W2 marked in Figure 1(a), the measured pulses arrive later than the simulated ones with a roughly constant offset. This is possibly attributed to W1 and W2 being erroneously positioned slightly to the left. This error also to some extent explains that the amplitude of the first arrival in the measurement is almost same as the second arrival, resulting from R1 being actually shadowed to an NLOS position by the top edge of W2. The third and onward arrivals of both the measurement and simulation are weaker than the first and second arrivals owing to geometric attenuation. In the right panel of the figure is the cumulative SPLs of the corresponding waveforms. In both of the measurement and simulation, the first and second arrivals contain most of the total energy. Aside from the difference caused by the aforementioned temporal and amplitude discrepancies of the waveforms, a good match is observed.

The left panel of Figure 5(b) plots the waveforms observed at R2, which is at an NLOS-1 position due to the top edge of W2. The waveforms are more complex than those at R1 owing to late arrivals. A notable difference from R1 is that the amplitudes of later arrivals can be same or even larger than first arrivals because the diffraction angles get shallower as the numbers of multiple reflections between W1 and W2 increases. The effect in a multiple reflection scenario is reported in (1, 4) and seen clearer in the measurement waveform of Figure 5(b). Like R1, the second and onward arrivals of the measured waveform are later than the simulated ones. However, the arrivals at 0.4 – 0.5 s are precise matches between the measurement and simulation. These arrivals are reflections by building wall W3 marked in Figure 1(a). From the accuracy of the arrivals, one can see that the total length of the propagation path is accurate. Furthermore, looking at the waveforms closely, it is noticed that there is a small arrival immediately behind the first arrival. The arrival is caused by reflection at building wall W4 of Figure 1(a), and then diffraction by the top edge of W2. The right panel of the figure shows the cumulative SPLs of the corresponding waveforms. Despite of the NLOS-1 position, the temporal histories of the measurement and simulation are an excellent match.

Figure Figure 5(c) plots the waveforms and cumulative SPLs observed at R3, which is an NLOS-1 position but with a longer diffracted path than R2. The amplitudes of the first four arrivals clearly increase in the measured waveform, in contrast to the measured waveform of R2. The increase is because geometric attenuation of late arrivals is less significant due to longer propagation path than R2. On the other hand, the effect is not clear in the simulated waveform. Instead, each pulse is stretched along temporal direction. This is possibly because of numerical dispersion inherent in the FDTD simulation. Reflection from W3 is not so clear compared to R2 because R3 is out of the reflected path.

3.3 R4–R8

Receivers R4–R8 are positioned in a row with a uniform spacing to study the effect of the number of diffractions by LOS, NLOS-1, and shallow NLOS-3 conditions. Figure 6 shows the waveforms and cumulative SPLs observed at R4–R8. The color scheme is same as Figure 5 with an addition of pale blue background, which indicates NLOS-3 propagation.

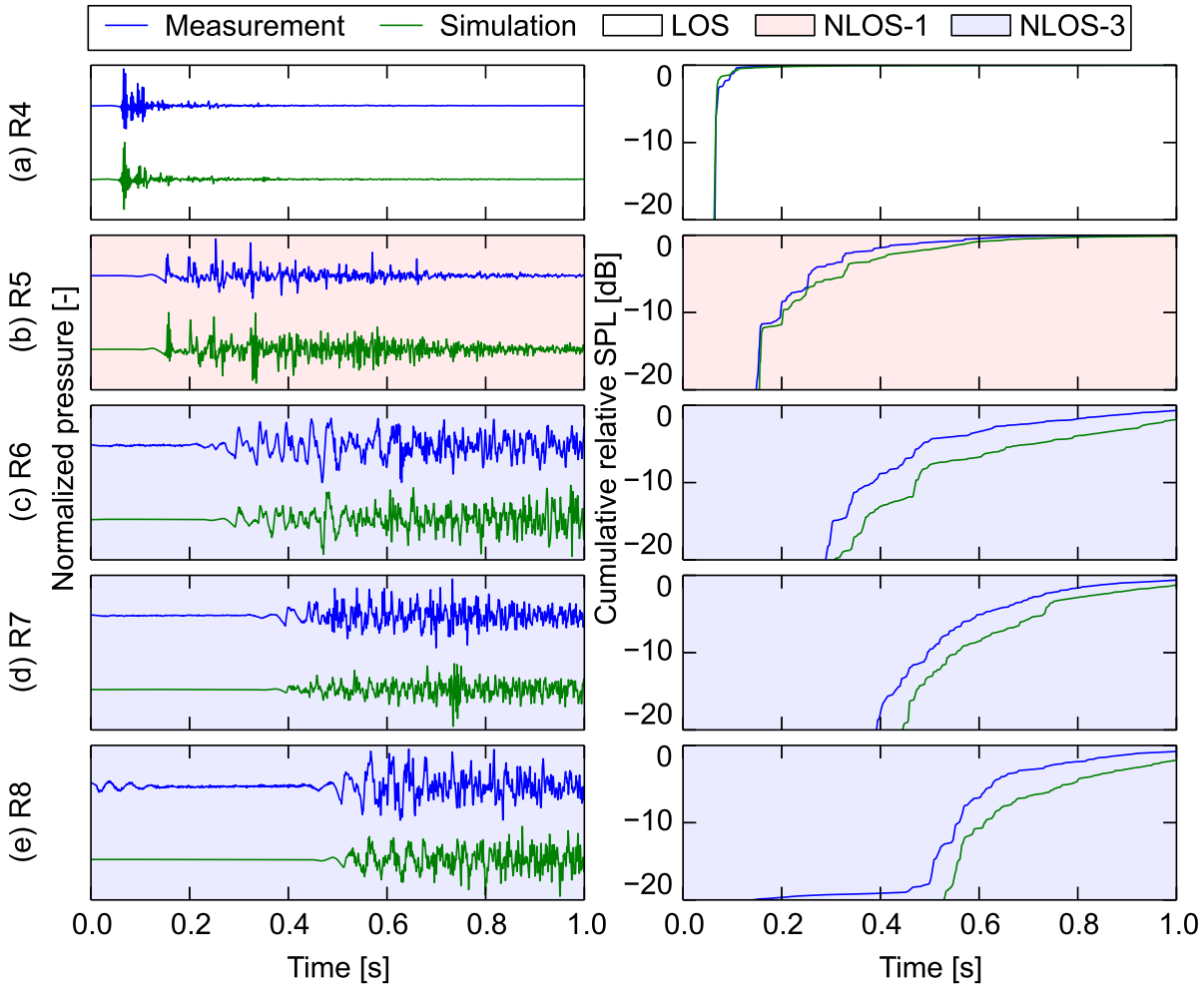

Figure 6 – (Left) waveforms and (right) cumulative relative SPLs at R4–R8.

Figures 6(a) and (b) shows observations at R4 and R5, which are at LOS and NLOS-1 positions respectively. The observations mostly follow R1–R3, with an exception of more complex arrivals observed at R5 owing to reflections from building wall W5 marked in Figure 1(a) and diffraction-reflection paths by the top edge of W6 of Figure 1(a) and the canyon enclosed by W5 and W6. The cumulative SPL curves of the measurement and simulation are a fairly good match but with a small difference.

Figure 6(c)–(e) are for R6–R8, respectively, which are at NLOS-3 positions due to triple diffractions by the top edges of W1, W5, and W7 marked in Figure 1(a). The third diffractions are relatively shallow because the receivers are positioned at the height near the top of W7. Nonetheless, the waveforms are clearly different and have more complex structure from those of R5 (NLOS-1). At R6, initial arrivals until approximately 0.5 s are elongated pulses rather than sharp pulses seen at LOS or NLOS-1 positions. The elongation is caused by multiple diffractions which work as low-pass filters (1). In contrast, later arrivals have notably higher frequency components. These pulses which begin to reach at approximately 0.5 s have gone through a flanking propagation path P1 marked in Figure 1(a) and diffracted by the side edge of W7. Pulses which reach at 0.6 s and onwards have gone through P1 and reflected by building wall W8 marked in Figure 1(a). Finally, pulses which have gone through flanking path P2 in Figure 1(a) reflect at W9 and reach R6. At R7 and R8, the pulses which have gone through NLOS-3 path and P1 flanking path arrive at almost the same instant. By comparing the measured and simulated waveforms, the initial elongated pulses are an excellent match, which reflects a general fact that simulation is especially good at predicting low-frequency wave propagation. In

contrast, the agreement of the late parts of the waveforms is not perfect. However, the simulation captures well the transition from elongated to complex late pulses. The waves at the beginning of the waveform at R8 is an artifact caused by signal processing.

Comparing the cumulative SPLs of R6–R8 between the measurements and simulation, the agreement is not so good. Specifically, in the simulation, the contribution of initial elongated pulses is smaller than the measurements and the total energy gradually increases over time.

3.4 R9–R11

Receivers R9–R11 are positioned to study the effects of multiple reflections and deep NLOS-3 conditions near the ground. Figure 7 shows the waveforms and cumulative SPLs observed at R9–R11. The color scheme is same as the previous figures with an addition of pale green background, which indicates NLOS-2 propagation.

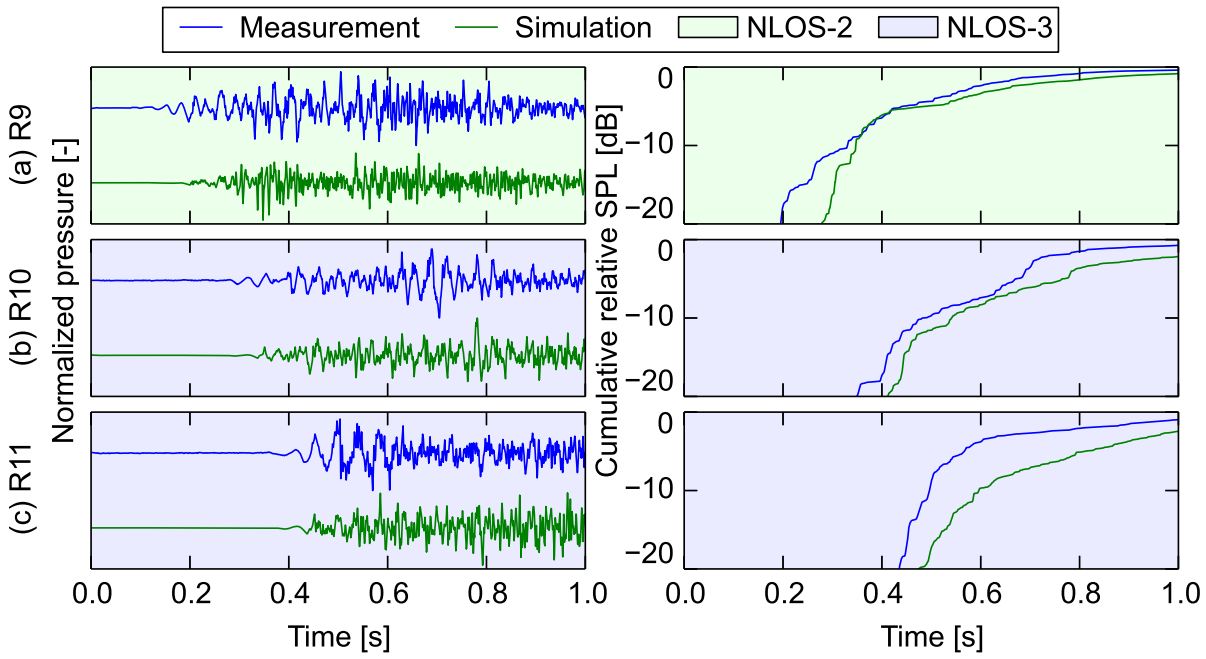

Figure 7 – (Left) waveforms and (right) cumulative relative SPLs at R9–R11.

The measured and simulated waveforms at R9 are shown in Figure 7(a). R9 is positioned between opposite walls W5 and W6 and at NLOS-2, which would in combination cause multiple reflections of elongated pulses. The measured waveform shows a series of elongated pulses. This is exactly expected from the topographical characteristics of the position. However, the simulated waveform does not exhibit the same behavior. This is possibly because pulses which have gone through P1 by multiple reflections, rather than diffractions, is stronger in the simulation because surfaces are assumed to be rigid.

The measured and simulated waveforms at R10 and R11 are shown in Figure 7(b) and (c), respectively. The receivers are considered to be most difficult points to measure or simulate, owing to the deep NLOS-3 condition and shielding by the W7 building. At R10, agreement of overall measured and simulated waveforms are relatively good. An elongated pulse right before 0.8 s is clearly visible both in the measurement and simulation. However, another elongated pulse at approximately 0.7 s in the measured waveform is not clearly visible in the simulation. At R11, elongated pulses of the initial arrivals in the measured waveform is not clearly visible in the simulation.

Comparing the cumulative SPLs of R9–R11 between the measurements and simulation, again, the agreement is not so good. Observations for R6–R8 in the previous subsection apply to R9–R11 as well.

3.5 R12–R15

Receivers R12–R15 are positioned in a row with a uniform spacing to study the effect of the depths of the diffractions in NLOS-1, 2, and 3 conditions. In this case, the depths is a combination of the number of diffractions and the diffraction angles in NLOS-3 conditions. Figure 8 shows the waveforms and cumulative SPLs observed at R12–R15.

The overall observation follows the previous observations. At R12, which is an NLOS-1 position, both the arrivals of the waveforms and the cumulative SPLs are excellent matches. As the depth gets deeper, the

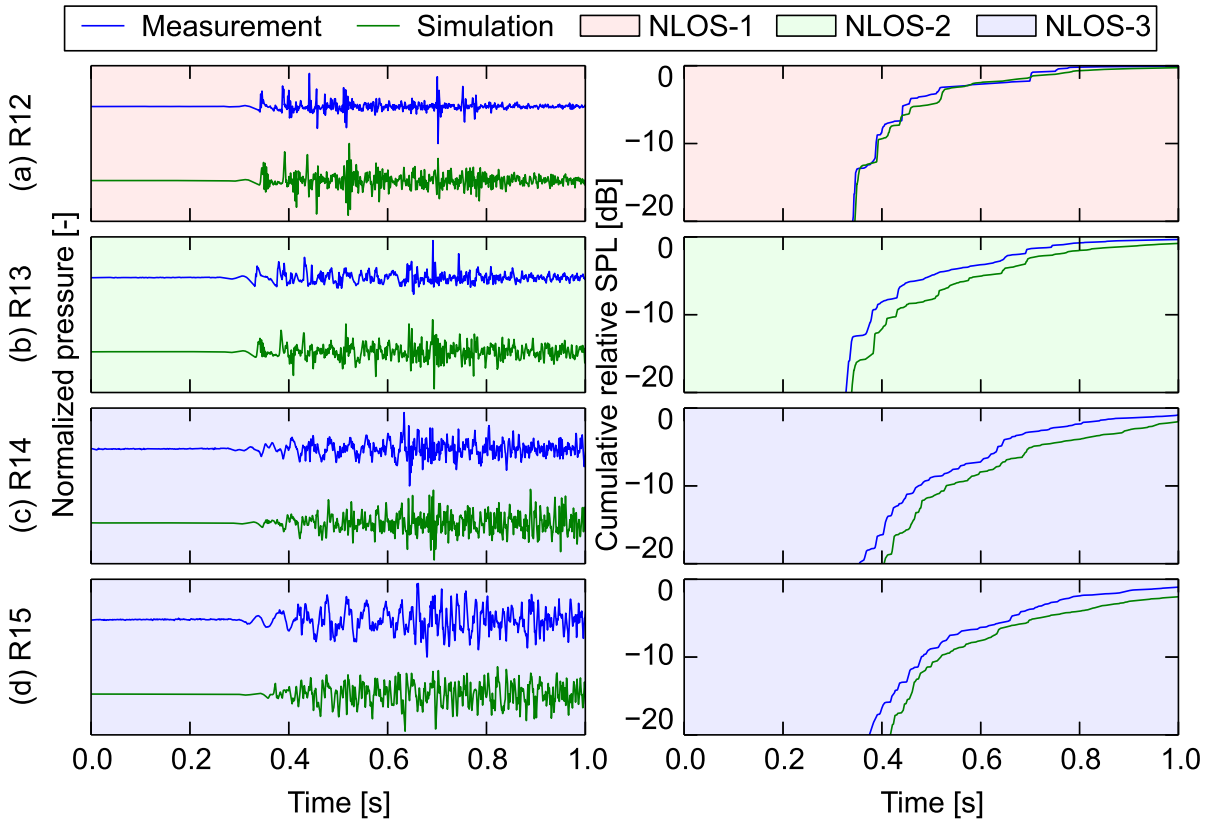

Figure 8 – (Left) waveforms and (right) cumulative relative SPLs at R12–R15.

similarities of the waveforms and cumulative SPLs reduce. Nonetheless, it is remarkable that a sharp (high-frequency) pulse at approximately 0.7 s seen in the measured and simulated waveforms of R12–R14 are excellent matches in spite of the long traveling time. The propagation path of this arrival is diffracted by the top edge of W2, reflected by W3, and further diffracted by W5 and W7 depending on the receiver positions.

4. CONCLUSIONS

In this paper, waveforms were compared between scale-model measurements and a FDTD simulation of outdoor acoustic pulse propagation over a real-life urban topography of a $380 \times 380\,\mathrm{m}^2$ area. For LOS and NLOS-1 positions, the arrival times of the propagated pulse and cumulative SPLs are excellent matches, except for small differences possibly caused by a geometrical error of the scale model. Even a long propagation of a reflected pulse that arrives in 0.7 s agreed. However, at NLOS-2 and NLOS-3 positions, agreement was not so good between the measurements and the simulation especially at deep diffraction and multiple reflection positions. Early arrivals of low-frequency pulses are not clear and cumulative SPLs in the simulation are weaker at early times in the simulation. Possible explanations are that (1) the rigid surface condition in the simulation exaggerated the reflected pulses compared to the measurements especially in multiple reflection scenarios and (2) the lack of air absorption correction weakened late reflected pulses in the measurements.

Some of the characteristics of complex urban propagation obtained in this study, such as the low-pass filter effect of diffraction propagation, are reported by (1, 4). However, with precisely controlled scale-model experimental conditions and larger domain size of this study ($150 \times 150\,\mathrm{m}^2$ (1, 4) versus $380 \times 380\,\mathrm{m}^2$), the effects are proved to be seen with more clarity even in more complex waveforms. The matched sharp pulse at 0.7 s of R12–R14 augments the applicability of wave-based simulation technique to study sound propagation over real-life complex urban topography.

ACKNOWLEDGEMENTS

This work was supported by JSPS Grant-in-Aid for Scientific Research (B) 23360255, Joint Usage/Research Center for Interdisciplinary Large-scale Information Infrastructures and Center for Spatial Information Science, the University of Tokyo. Parts of the fundamental geospatial data by the Geospatial Information Authority of Japan were used.

REFERENCES

1. Albert DG, Liu L. The effect of buildings on acoustic pulse propagation in an urban environment. J Acoust Soc Am. 2010 March;127(3):1335–1346.

2. Heimann D. Wide-area assessment of topographical and meteorological effects on sound propagation by time-domain modeling. J Acoust Soc Am. 2013 May;133(5):EL419–EL425.

3. Oshima T, Imano M, Hiraguri Y, Kamoshida Y. Linearized Euler simulations of sound propagation with wind effects over a reconstructed urban terrain using digital geographic information. Appl Acoust. 2013 December;74(12):1354–1366.

4. Mehra R, Raghuvanshi N, Chandak A, Albert DG, Wilson DK, Manocha D. Acoustic pulse propagation in an urban environment using a three-dimensional numerical simulation. J Acoust Soc Am. 2014 June;135(6):3231–3242.

5. Oshima T, Ishizuka T, Kamijo T. Scale-model validation study of finite-difference time-domain simulations over a real-life area reconstructed with digital geographic information. Proc Inter-Noise 2013. 2013 September;(1025):10 pages.

6. Albert DG, Liu L, Moran ML. Time reversal processing for source location in an urban environment. J Acoust Soc Am. 2005 August;118(2):616–619.

7. Oshima T, Ishizuka T, Kamijo T. Three-dimensional urban acoustic simulations and scale-model measurements over real-life topography. J Acoust Soc Am. 2014 June;135(6):EL324–EL330.

8. Kokusai Kogyo Co , Ltd . RAMS-e surface; Retrieved 2, April 2012. http://www.ramse3d.com/laser/lib/index.html.

9. Zenrin Co , Ltd . Zmap-TOWNII; Retrieved 2, April 2012. http://www.zenrin.co.jp/product/gis/zmap/zmaptown.html.

10. Oshima T, Hiraguri Y, Imano M. Geometry reconstruction and mesh generation techniques for acoustic simulations over real-life urban areas using digital geographic information. Acoust Sci Technol. 2014;35(2):108–118.

11. Qui Q, Geers TL. Evaluation of the perfectly matched layer for computational acoustics. J Comput Phys. 1998;139:166–183.